

Temporal interference driven by an oscillating electric field in photodetachment of H^- ion

De-Hua Wang(王德华), Meng-Zhi Li(李梦芝), Hong-Na Song(宋鸿娜), Xiao-Xiao Ren(任笑笑)
Citation: Chin. Phys. B . 2018, 27(2): 023202. **doi:** 10.1088/1674-1056/27/2/023202

Journal homepage: http://cpb.iphy.ac.cn; http://iopscience.iop.org/cpb

What follows is a list of articles you may be interested in

Photodetachment dynamics of H^- ion in a harmonic potential plus a time-dependent oscillating electric field

De-Hua Wang(王德华), Chuan-Juan Wang(王传娟)
Chin. Phys. B . 2017, 26(10): 103202. **doi:** 10.1088/1674-1056/26/10/103202

Quantum and semiclassical studies on photodetachment cross sections of H^- in a harmonic potential

Hai-Jun Zhao(赵海军), Wei-Long Liu(刘伟龙), Meng-Li Du(杜孟利)
Chin. Phys. B . 2016, 25(3): 033203. **doi:** 10.1088/1674-1056/25/3/033203

Photodetachment of H^- near a hard wall with arbitrary laser polarization direction

Azmat Iqbal, A. Afaq
Chin. Phys. B . 2015, 24(8): 083201. **doi:** 10.1088/1674-1056/24/8/083201

Electron flux distributions in photodetachment of HF^- near an interface: theoretical imaging method study

Maryam Nawaz Awan, A. Afaq
Chin. Phys. B . 2013, 22(1): 013205. **doi:** 10.1088/1674-1056/22/1/013205

Temporal interference driven by an oscillating electric field in photodetachment of H^- ion*

De-Hua Wang(王德华)†, Meng-Zhi Li(李梦芝), Hong-Na Song(宋鸿娜), and Xiao-Xiao Ren(任笑笑)

School of Physics and Optoelectronic Engineering, Ludong University, Yantai 264025, *China*

(Received 20 September 2017; revised manuscript received 27 November 2017; published online 5 January 2018)

The real time domain interferometry for the photodetachment dynamics driven by the oscillating electric field has been studied for the first time. Both the geometry of the detached electron trajectories and the electron probability density are shown to be different from those in the photodetachment dynamics in a static electric field. The influence of the oscillating electric field on the detached electron leads to a surprisingly intricate shape of the electron waves, and multiple interfering trajectories generate complex interference patterns in the electron probability density. Using the semiclassical open-orbit theory, we calculate the interference patterns in the time-dependent electron probability density for different electric field strengths, different frequencies and phases in the oscillating electric field. This method is universal, and can be extended to study the photoionization dynamics of the atoms in the time-dependent electric field. Our study can guide the future experimental researches in the photodetachment or photoionization microscopy of negative ions and atoms in the oscillating electric field.

Keywords: temporal interference, photodetachment dynamics, oscillating electric field, semiclassical open-orbit theory

PACS: 32.80.Gc, 31.15.xg **DOI:** 10.1088/1674-1056/27/2/023202

1. Introduction

In the microscopic field, the quantum description of atoms and molecules is based on the wave function. In the past, the information about the wave function of the microscopic particle was by means of comparing some observables that can be calculated theoretically and can be measured in experiments, such as the photoabsorption of atom or molecule in the external fields. Based on the photodetachment experiment, the electron imaging techniques make the observation of the wave function become possible. In the early 1980s, Demkov *et al.* first introduced the principle of photodetachment microscopy.[1–3] They found the photodetachment of a negative ion in the static electric field, the detached electron trajectory is analogous to a parabola. Two electron trajectories could reach a detector point perpendicular to the electric field, which leads to an interference pattern in the electron flux distribution. This predication was experimentally realized after the emergence of photoelectron imaging techniques.[4–6] Using this technique, people can precisely measure the electron affinities in the negative ion.[7–13] In the theoretical aspect, Du put forward a semiclassical method for studying the interference pattern in the photodetachment of H^- ion in an electric field.[14] Later, it was developed into studying the photodetachment of the negative ion in the coexistence of electric and magnetic fields.[15–22] In 2010, Zhao and Delos put forward a semiclassical open-orbit theory to study the photoionization microscopy of a Rydberg hydrogen atom in a static electric field.[23] Recently, Yang and Robicheaux *et al.* extended this semiclasical method to the time-dependent electric field and studied the phtodetachment dynamics of negative ions in the time-dependent electric field.[24–30] Inspired by these previous works, in this paper, we extend the semiclassical open-orbit theory to the time-dependent electric field and study the interference effect in the photodetachment of H^- ion in an oscillating electric field. It is found that this system is quite different from the case in a static electric field. The photo-detached electron can follow multiple trajectories to arrive at the detector. Therefore, a complex interference pattern in the electron probability density will appear on the detector in contrast to the regular two-term interference pattern in the static electric field. In addition, the electron probability density on the detector is time-dependent. Our study provides an opportunity to observe electron interference in the real time domain and may guide the future experiments for exploring the photodetachment microscopy in the time-dependent electric field.

2. Photodetached electron motion in an oscillating electric field

For the photodetachment of an H^- ion, we use the laser light field linearly polarized along the z axis with the following form[24]

$$f_{\mathrm{L}}(t) = \frac{1}{2}\left[\tanh\left(\frac{t-t_{\mathrm{u}}}{\Delta t_{\mathrm{L}}}\right) - \tanh\left(\frac{t-t_{\mathrm{d}}}{\Delta t_{\mathrm{L}}}\right)\right], \qquad (1)$$

*Project supported by the National Natural Science Foundation of China (Grant No. 11374133) and the Taishan Scholars Project of Shandong Province, China (Grant No. ts2015110055).

†Corresponding author. E-mail: lduwdh@163.com

© 2018 Chinese Physical Society and IOP Publishing Ltd

where t_u, t_d and Δt_L are the laser light field parameters. In this work, we choose $t_d = -t_u = 3.14$ ps, $\Delta t_L = 0.23$ ps. The external driving oscillating electric field is $F(t) = F_0 \sin(\omega t + \varphi)$. Where F_0 is the amplitude, ω is the frequency, and φ denotes the phase. Both the laser field and the oscillating electric field are along the z axis. The H^- ion is localized at the origin, with a detector plane placed at the $z = -z_0$ plane. Since the electric field oscillates with time, we extend the phase space by including the time t and its conjugate momentum p_t. Then the Hamiltonian describing the electron motion in the oscillating electric field can be written as (using the cylindrical coordinates (ρ, z, ϕ))[27]

$$\begin{aligned} &H(\rho, z, t, p_\rho, p_z, p_t) \\ &= \frac{1}{2}p_\rho^2 + \frac{1}{2}p_z^2 + F_0 \sin(\omega t + \varphi) z + p_t. \end{aligned} \tag{2}$$

In the augmented space, we add two motion equations: $\mathrm{d}t/\mathrm{d}\tau = 1$, $\mathrm{d}p_t/\mathrm{d}\tau = -\partial H/\partial t$. Here, τ is the evolution time for the electron trajectory in the oscillating electric field: $\tau = t - t_i$. By solving the Hamiltonian canonical equations with the negative ion centered at the origin combined with the initial conditions: $t(\tau = 0) = t_i$, $p_t(\tau = 0) = -E$, we obtain the classical motion equations of the detached electron in the oscillating electric field[27]

$$\begin{cases} \rho(t) = k_0 \sin\theta_i (t - t_i), \\ z(t) = \left[k_0 \cos\theta_i - \dfrac{F_0}{\omega}\cos(\omega t_i + \varphi)\right] \cdot (t - t_i) \\ \qquad + \dfrac{F_0}{\omega^2}[\sin(\omega t + \varphi) - \sin(\omega t_i + \varphi)], \end{cases} \tag{3}$$

where k_0 is the initial momentum of the detached electron, $k_0 = \sqrt{2E}$. θ_i is the initial outgoing angle of the detached electron relative to the $+z$ axis.

According to the semiclassical open-orbit theory,[23] after the electron is photodetached from the negative ion, it will travel in the form of an outgoing wave along a classical trajectory. Under the influence of the oscillating electric field, multiple electron trajectories can reach the detector simultaneously. The interference effect between these electron waves causes the oscillatory structures in the electron probability density on the detector. Suppose the detector is localized at the point $\{\rho(t) = 0, z(t) = -z_0\}$. From Eq. (3), we can find out the electron trajectory emitted from the origin and finally arriving at the detector. Let $\rho(t) = 0$, i.e., $k_0 \sin\theta_i (t - t_i) = 0$, we get $\theta_i = 0$ or $\theta_i = \pi$, which means only the electron trajectory emitted along the z axis can reach the detector. If the electron trajectory is emitted with the outgoing angle $\theta_i = 0$, we call it the up orbit; while the electron trajectory with the outgoing angle $\theta_i = \pi$ is called the down orbit.

Let $z(t) = -z_0$

$$\left[k_0 \cos\theta_i - \frac{F_0}{\omega}\cos(\omega t_i + \varphi)\right] \cdot (t - t_i) + \frac{F_0}{\omega^2}[\sin(\omega t + \varphi) - \sin(\omega t_i + \varphi)] = -z_0. \tag{4}$$

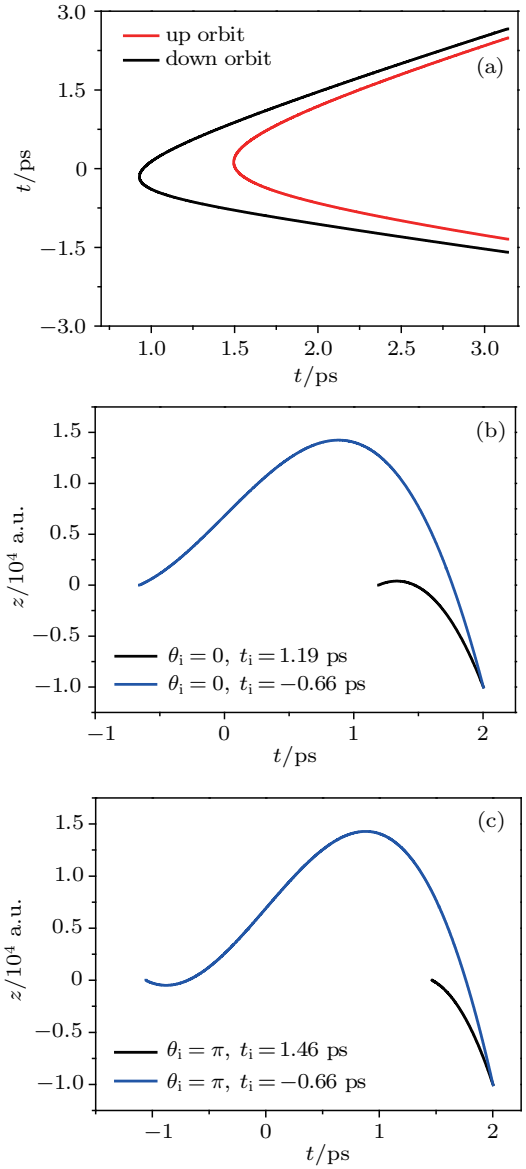


Fig. 1. (color online) (a) The t–t_i curve that the detached electron can reach the detector. The photon energy $E_p = 1.0$ eV, the oscillating electric field parameters are as follows: $F_0 = 200$ kV/cm, $\omega = 1.21 \times 10^{-5}$ a.u., $\varphi = 0$. The detector is localized at the point ($\rho = 0$, $z = -10^4$ a.u.). The black line represents the down orbit and the red line denotes the up orbit. (b) Two up orbits of the detached electron which are emitted from the origin and arrive at the detector at the same final time $t = 2.0$ ps. (c) Two down orbits of the detached electron arrived at the detector at the same final time $t = 2.0$ ps.

By solving the above equation, we can obtain the initial time t_i and the final time t for each electron trajectory that can reach the detector. Suppose the photon energy $E_p = 1.0$ eV, the oscillating electric field parameters are as follows: $F_0 = 200$ kV/cm, $\omega = 1.21 \times 10^{-5}$ a.u., $\varphi = 0$. The detector is localized at the point $\{\rho = 0,\ z = -10^4$ a.u.$\}$. Figure 1(a) depicts the t–t_i curve that the electron can reach the detector. From this plot, we find the t–t_i curve can be divided into two parts. In the first part, 0.92 ps $< t <$ 1.49 ps, only two down orbits can arrive at the detector. However, in the second part, 1.49 ps $\leq t <$ 3.14 ps, four electron trajectories can

reach the detector, two up orbits plus two down orbits. Figure 1(b) shows two up orbits of the detached electron which emitted from the origin and arrived at the detector. Although they reach the detector at the same final time t, their initial outgoing times t_i are different. The black line denotes the electron trajectory emitted at the initial time $t_i = 1.19$ ps, and the blue line is the orbit emitted at the initial time $t_i = -0.66$ ps. In Fig. 1(c), we show two down orbits of the detached electron that can reach the detector at the same final time. One is emitted at the initial time $t_i = -1.07$ ps, and the other is emitted at $t_i = 1.46$ ps.

3. The time-dependent detached electron probability density

As the electron moves far away from the hydrogen atom, we can use the semiclassical approximation to construct the electron wave function. At a given point $M(\rho, -z_0)$ on the detector, the wave function can be written as

$$\psi_f(\rho, -z_0, t) = \sum_{i=1}^{n} f_L(t_i)\psi_{out}(R, \theta_i, \varphi_i)A_i e^{i[S_i - \mu_i\pi/2 - Et_i]}, \quad (5)$$

where $\psi_{out}(R, \theta_i, \varphi_i)$ is the outgoing electron wave function from a spherical surface with a small radius R[14]

$$\psi_{out}(R, \theta_i, \varphi_i) = \frac{4B_0 k i}{(k_b^2 + k^2)^2} \frac{e^{ikR}}{R} \cos\theta_i. \quad (6)$$

Here $k_b = \sqrt{2E_b}$, $E_b = 0.754$ eV is the binding energy of the H^- ion and $B_0 = 0.31552$ is a constant.

The summation in Eq. (5) includes all the electron orbits reaching the detector at the same final time t. A_i is the semiclassical amplitude:

$$A_i = \left| \frac{J_i(\tau = 0)}{J_i(\tau = t - t_i)} \right|^{1/2}, \quad (7)$$

$J(\tau)$ is the Jacobian[24]

$$J(\tau) = \rho(t) \det\left(\frac{\partial(\rho, z, t)}{\partial(t_i, \theta_i, \tau)} \right). \quad (8)$$

Using the classical motion equations of the detached electron, we obtain

$$A_i = \frac{R}{k_0(t - t_i)} \left| \frac{k_0}{k_0 - F_0 \sin(\omega t_i + \varphi)\cos\theta_i (t - t_i)} \right|^{1/2}, \quad (9)$$

S_i is the classical action along the i-th trajectory[25]

$$S = \int p\,dq = \int_{t_i}^{t} p_\rho\,d\rho + \int_{t_i}^{t} p_z\,dz + \int_{t_i}^{t} p_t\,dt, \quad (10)$$

μ_i is the Maslov index for the i-th trajectory, which equals the number of the singular points along the trajectory.

The electron probability density at a given point $M(\rho, -z_0)$ on the detector is

$$P(\rho, -z_0, t) = |\psi_f(\rho, -z_0, t)|^2. \quad (11)$$

Substituting Eq. (5) into the above equation, we obtain

$$P(\rho, -z_0, t) = \sum_i |\psi_i|^2 + \sum_{i<j} \mathrm{Re}(\psi_i \psi_j^*)\cos(\chi_i - \chi_j), \quad (12)$$

where

$$\psi_i = f_L(t_i)\frac{4B_0 k\cos\theta_i}{(k_b^2 + k^2)^2 R} A_i, \quad \chi_i = S_i - Et_i - \mu_i\pi/2.$$

4. Results and discussions

Using Eq. (12), we calculate the detached electron probability density on the detector in the oscillating electric field. Since the electron probability density on the detector depends on the photon energy, the initial outgoing time t_i and the final time t of the detached electron are sensitive. In this work, we choose the photon energy $E_p = 1.0$ eV and calculate the electron probability density distribution in the time interval $[-3.14, 3.14]$ ps.

Firstly, we study the influence of the oscillating electric field strength on the electron probability density distribution. The frequency and phase in the oscillating electric field are: $\omega = 1.21 \times 10^{-5}$ a.u., $\varphi = 0$. The detector is localized at the point $\rho = 0$, $z = -10^4$ a.u. Figure 2(a) shows the t–t_i curve for the detached electron in the oscillating electric field with the electric field strength $F_0 = 20$ kV/cm. Under this condition, only two down orbits can reach the detector at the same final time. Due to the interference effect between these two orbits, oscillatory structures appear in the electron probability density, as we can see from Fig. 2(b). Figure 2(c) shows the t–t_i curve with the electric field strength $F_0 = 40$ kV/cm, we find except for the two down orbits, the two up orbits of the detached electron begin to appear. However, the up orbits only appear at the final time $t = 2.94$ ps. In the region 1.20 ps $< t <$ 2.94 ps, only two down orbits can arrive at the detector; however, in the region 2.94 ps $\le t <$ 3.14 ps, four detached electron orbits can reach the detector. Figure 2(d) shows the electron probability density distribution on the detector with the oscillating electric field strength $F_0 = 40$ kV/cm. It is found that the oscillatory structure in the electron probability density distribution is divided into two segments by the boundary time ($t = 2.94$ ps) as shown in the t–t_i curve. In the first interval 1.20 ps $< t <$ 2.94 ps, the electron probability density exhibits an approximately two-term oscillatory pattern. In the second interval 2.94 ps $\le t <$ 3.14 ps, the oscillatory structure in the electron probability density becomes much more complex due to the interference effect of the four electron orbits arriving at the detector at the same final time. As we

further increase the oscillating electric field strength, the final time that the up orbits begin to appear decreases. For example, in Fig. 2(e), for the electric field strength $F_0 = 60$ kV/cm, the final time that the up orbits begin to appear is decreased to $t = 2.46$ ps. We find the corresponding electron probability density gets complicated as the final time $t \geq 2.46$ ps, which is shown in Fig. 2(f). As the electric field strength is increased to $F_0 = 500$ kV/cm, the effect of the oscillating electric field force becomes stronger. After a small period of time, the electron will reach the detector. The whole t–t_i curve is dominated by four electron orbits, only in a small interval $0.73\ \text{ps} \leq t < 1.06$ ps can two orbits exist, as shown in Fig. 2(i). Figure 2(j) is the electron probability density with the electric field strength $F_0 = 500$ kV/cm, where we find that the oscillatory structures get much more complicated and the two-term oscillatory structure only appears in a small region.

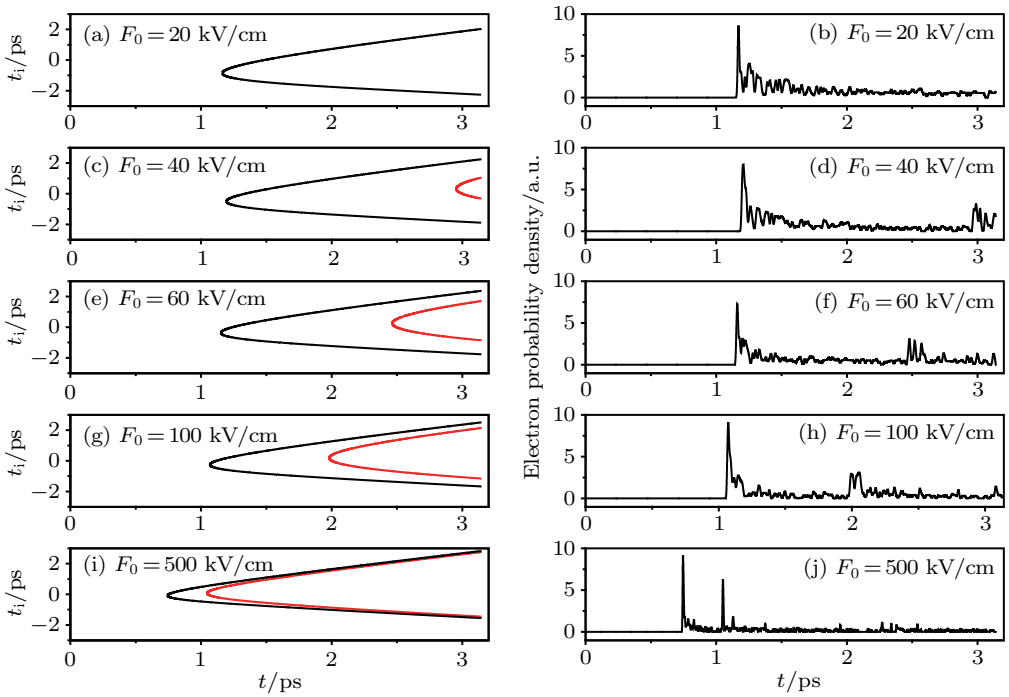


Fig. 2. (color online) The t–t_i curve and the electron probability density on the detector for the photodetachment of the H^- ion in the oscillating electric field with different electric field strength. The oscillating electric field frequency $\omega = 1.21 \times 10^{-5}$ a.u. and the phase $\varphi = 0$. The detector is localized at the point $\rho = 0, z = -10^4$ a.u. The black line represents the down orbit and the red line denotes the up orbit. The left column is the t–t_i curve that the detached electron can reach the detector, while the right column is the corresponding electron probability density on the detector. The electric field strength is denoted in each plot.

Next, we show how the electron probability density on the detector varies with the oscillating electric field frequency ω, suppose $F_0 = 200$ kV/cm, $\varphi = 0$. In Fig. 3(a), we plot the t–t_i curve with $\omega = 2.42 \times 10^{-5}$ a.u. We can see that the final time t is always larger than 0. In addition, the t–t_i curve is divided into two segments by a boundary time $t = 1.16$ ps. Figure 3(b) is the corresponding time-dependent electron probability density distribution on the detector. It is found in the region $0.78\ \text{ps} < t < 1.16$ ps, an approximately two-term oscillatory structure appears in the electron probability density. However, in the interval $1.16\ \text{ps} \leq t < 3.12$ ps, four detached electron trajectories can arrive at the detector, which causes the electron probability density to get complex. Figure 3(c) shows the t–t_i curve with $\omega = 4.84 \times 10^{-5}$ a.u. We can see that the final time t is extended to the region $t < 0$. The final time t for the up orbits and the down orbits are extended to two regions. To be more exact, the up orbits lie in the regions $0.94\ \text{ps} < t < 2.34$ ps and $-2.22\ \text{ps} < t < -1.11$ ps; the down orbits lie in the regions $0.66\ \text{ps} < t < 2.15$ ps and $-2.47\ \text{ps} < t < -1.13$ ps. The time-dependent electron probability density distribution on the detector with $\omega = 4.84 \times 10^{-5}$ a.u. is given in Fig. 3(d). We find that the oscillatory structures in the electron probability density distribution can be divided into approximately three intervals. In the first interval, $-2.47\ \text{ps} < t < -1.11$ ps, the oscillatory structure is caused by one up orbit and one down orbit. In the second interval, $0.66\ \text{ps} < t < 0.96$ ps, the oscillatory structure is caused by two down orbits. However, in the third interval, $0.96\ \text{ps} < t < 2.33$ ps, the oscillatory structure in the electron probability density is caused by the interference effect between four detached electron's orbits. With the increase of the frequency ω, the effect of the oscillating electric field force becomes significant. More electron trajectories can arrive at a given point on the detector, which induces a much more complex oscillatory structure in the electron probability density. For example, in Figs. 3(e)–3(f), the electric field frequency $\omega = 6.05 \times 10^{-5}$ a.u., the t–t_i curve and the electron probability density distribution on the detector can be divided into four regions. In the first and third re-

gions, -1.88 ps $< t < -1.62$ ps and 0.64 ps $< t <$ 0.89 ps, two down orbits can arrive at the detector, which causes the oscillatory structure in the electron probability density distribution. In the second region, -1.62 ps $< t < -0.81$ ps, two down orbits and two up orbits can arrive at the detector, the interference between these four orbits leads to the oscillation in the electron probability density distribution. In the last interval, 0.88 ps $< t <$ 1.73 ps, two down orbits and three up orbits can reach the detector at the same final time, which makes the oscillation in the electron probability density distribution get complicated. As the oscillating electric field frequency is increased to $\omega = 1.21 \times 10^{-4}$ a.u. (Figs. 3(k)–3(l)), the whole t–t_i curve and the electron probability density distribution on the detector can be divided into more segments. At some region, the number of the detached electron's orbit which can reach the detector is great. For instance, in the interval 2.01 ps $< t <$ 2.22 ps, 14 orbits can reach the detector, correspondingly, the electron probability density distribution on the detector becomes much more complex. The reason can be analyzed using the semiclassical open orbit theory. Since the oscillatory structure in the electron probability density distribution is caused by the interference between different electron orbits arriving at the same point on the detector, the greater the number of the electron orbits, the more electron waves can reach the detector, therefore, their interference effect in the electron probability density distribution becomes much stronger.

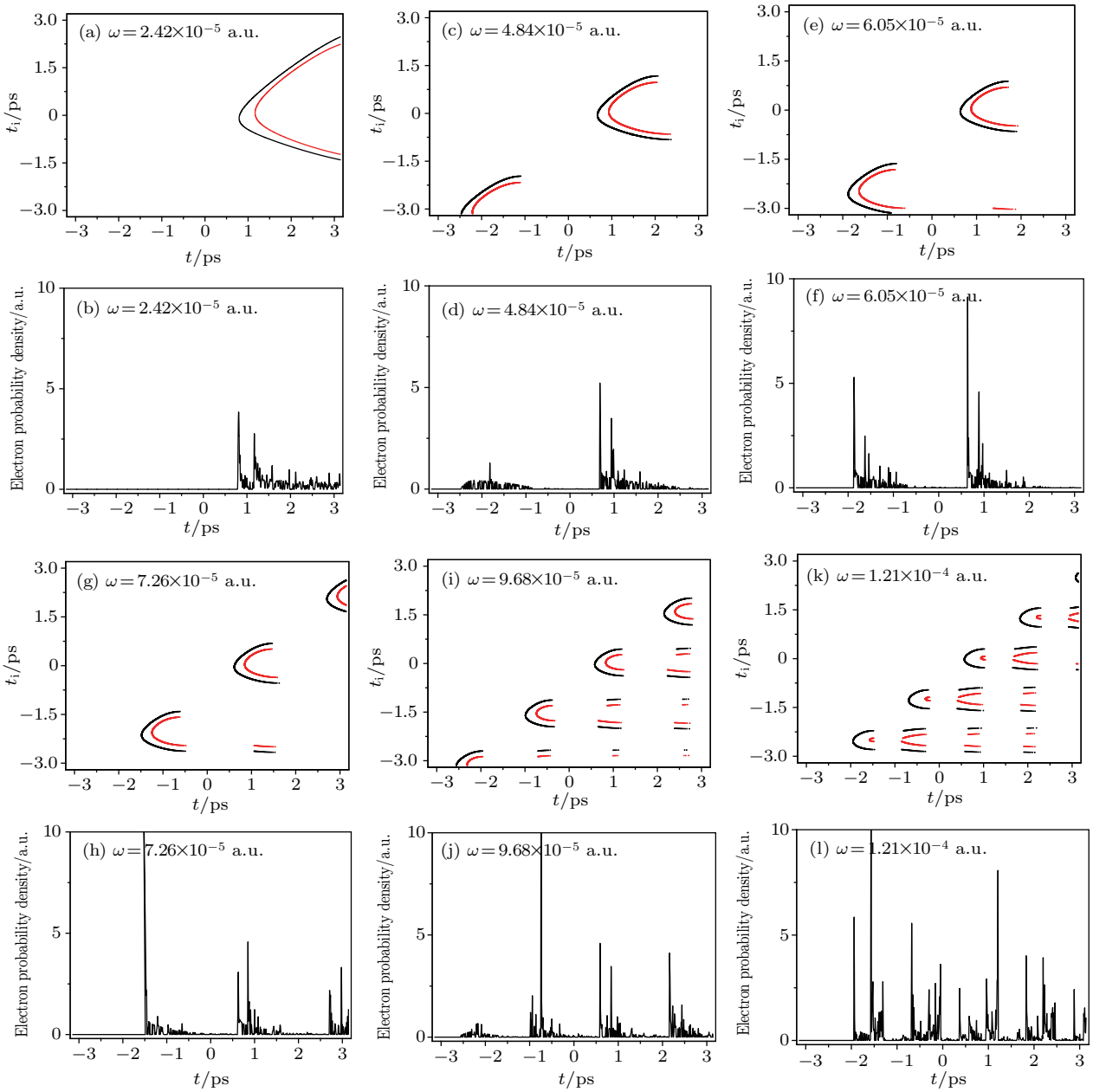


Fig. 3. (color online) Variation of the t–t_i curve and the electron probability density on the detector with the oscillating electric field frequency. $F_0 = 200$ kV/cm, $\varphi = 0$. The detector is localized at the point $\rho = 0$, $z = -10^4$ a.u. The black line represents the down orbit and the red line denotes the up orbit. Panels (a), (c), (e), (g), (i), and (k) are the t–t_i curves that the detached electron can reach the detector, while panels (b), (d), (f), (h), (j), and (l) are the corresponding electron probability densities on the detector. The oscillating electric field frequency is given in each plot.

In the following, we fix the oscillating electric field strength and frequency: $F_0 = 300$ kV/cm, $\omega = 2.42 \times 10^{-5}$ a.u. Then we discuss the influence of the phase φ in the oscillating electric field on the electron probability density. The result is shown in Fig. 4. Figure 4(a) shows the electron probability density with $\varphi = 0$. Under this condition, the final time that the detached electron can reach the detector is always positive, therefore, the oscillation in the electron probability density is localized in the region $t > 0$. Figure 4(b) is the case with the phase $\varphi = \pi/2$. We find the oscillating region in the electron probability density is expanded to the region $t < 0$. Figure 4(c) shows the electron probability density with $\varphi = \pi$. The oscillatory structure exhibits an approximately two-term interference pattern and is mainly localized in the region $t < 0$. The reason is as follows: as $\varphi = \pi$, the oscillating electric field becomes $F(t) = -F_0 \sin(\omega t)$, which is larger than 0 as $t < 0$. Therefore, the oscillating electric field is always pointing along the $+z$ axis in the region $t < 0$, correspondingly, the electric field force acting on the detached electron is along the $-z$ axis. When the electron is emitted along the $+z$ axis, the electric field force can decelerate the movement of the electron, then after a period of time, it will return back and reach the detector. However, when the electron travels along the $-z$ axis, the electric field force can accelerate the movement of the electron, after a small period of time, it will reach the detector. Therefore, when the phase $\varphi = \pi$, only two detached electron orbits can reach the detector at the same final time, which causes a two-term interference pattern in the electron probability density on the detector. As we further increase the phase $\varphi = 3\pi/2$, the electron probability density distribution on the detector can be divided into two regions, one is in the region with the final time -2.57 ps $< t < -1.15$ ps and another is in the region 2.34 ps $< t <$ 3.14 ps, as we can see from Fig. 4(d) clearly. From this figure, we conclude that the electron probability density on the detector sensitively depends on the phase in the oscillating electric field.

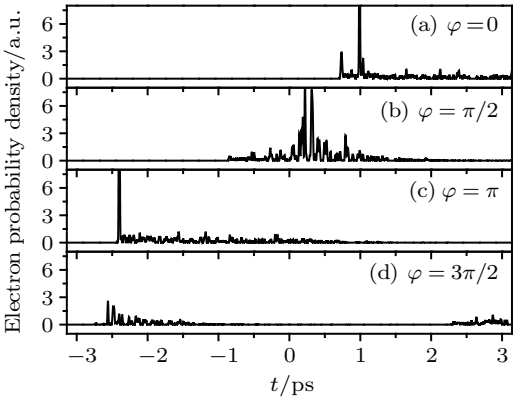


Fig. 4. Variation of the t–t_i curve and the electron probability density on the detector with the phase in the oscillating electric field. $F_0 = 300$ kV/cm, $\omega = 2.42 \times 10^{-5}$ a.u. The detector is localized at the point $\rho = 0$, $z = -10^4$ a.u. The phase in the oscillating electric field is given in each plot.

Finally, we discuss the variation of electron probability density with the position of the detector. The parameters in the oscillating electric field are as follows: $F_0 = 200$ kV/cm, $\omega = 2.42 \times 10^{-5}$ a.u., $\varphi = 0$. The detector is moved along the $-z$ axis, the distance from the detector to the origin is changed from 500 a.u. to 6000 a.u. We find that although the distance from the ion to the detector is different, the oscillatory structures in the electron probability density are similar. The electron probability density on the detector can be divided into two regions, one is caused by the interference between two electron orbits, while the other region is caused by the interference between four electron orbits. However, the oscillating amplitude and oscillating region are changed as we move the detector along the $-z$ axis.

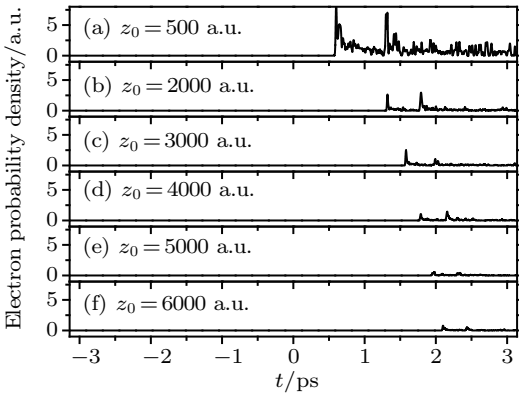


Fig. 5. Variation of the electron probability density in the oscillating electric field with the position of the detector. The parameters in the oscillating electric field are as follows: $F_0 = 200$ kV/cm, $\omega = 2.42 \times 10^{-5}$ a.u., $\varphi = 0$.

Figure 5(a) shows the electron probability density in the oscillating electric field with the detector localized at the point $\rho = 0, z = 500$ a.u. Under this condition, the oscillatory structure in the electron probability density is very complex. Both the oscillating amplitude and the oscillating region are very large. As we move the detector far away from the origin, both the oscillating amplitude and the oscillating region in the electron probability density become decreased. The oscillatory structure in the electron probability density gets weaker. For example, in Fig. 5(b), the distance from the detector to the origin is 2000 a.u., the oscillating structure is confined to the region 1.31 ps $< t <$ 3.14 ps. In Fig. 5(f), the detector is localized at $\rho = 0$, $z = 6000$ a.u., we can see that the oscillatory structure in the electron probability density is only limited in a small region 2.01 ps $< t <$ 3.14 ps. In addition, the oscillating amplitude becomes very small. The reason is as follows: when the detector is close to the origin, after the electron is emitted from the origin, it will reach the detector in a small period of time. From Eq. (9), we can see that the amplitude factor A for the electron orbit is very large, thus the contribution of the electron's orbit to the electron probability density is significant. As the detector is far away from the origin, it will take

quite a long time for the electron to reach the detector, which makes the amplitude factor of the electron orbit become small. Consequently, the oscillating amplitude in the electron probability density induced by the electron orbit is small and the oscillating region gets decreased.

5. Conclusion

The interference effect driven by an oscillating electric field in the photodetachment of the H^- ion has been studied. An analytical formula for calculating the electron probability density has been put forward based on the seimiclassical open-orbit theory. It is found that the oscillating electric field can cause multiple electron trajectories to reach the same point on the detector in contrast to the photodetachment of negative ion in the static electric field, where only two detached electron trajectories can reach the detector point. The interference effect between different electron trajectories generates complex interference patterns in the electron probability density. Our calculation results suggest that the interference patterns in the electron probability density can be controlled by changing the oscillating electric field parameters and the position of the detector. The semiclassical method used in this work provides a visual intuitive picture for the photodetachment dynamics in the oscillating electric field from a time-dependent viewpoint, and can be used to study the photodetachment of other multi-electron negative ions in the oscillating electric field, such as F^- ion, H_2^-, etc. Our study may guide the experimental research in the temporal interference for the photodetachment dynamics in the oscillating electric field.

References

[1] Demkov Yu N, Kondratovich V D and Ostrovsky V N 1981 *JETP Lett.* **34** 425
[2] Kondratovich V D and Ostrovsky V N 1984 *J. Phys. B: At. Mol. Phys.* **17** 1981
[3] Kondratovich V D and Ostrovsky V N 1984 *J. Phys. B: At. Mol. Phys.* **17** 2011
[4] Heck A J R and Chandler D W 1995 *Ann. Rev. Phys. Chem.* **46** 335
[5] Goldfarb F, Drag C, Chaibi W, Kroger S, Blondel C and Delsart C 2005 *J. Chem. Phys.* **122** 014308
[6] Blondel C, Chaibi W, Delsart C and Drag C 2005 *Eur. Phys. J. D* **33** 335
[7] Blondel C, Delsart C and Dulieu F 1996 *Phys. Rev. Lett.* **77** 3755
[8] Walter C W, Hertzler C F, Devynck P, Smith G P and Peterson J R 1991 *J. Chem. Phys.* **95** 824
[9] Valli C, Blondel C and Delsart C 1999 *Phys. Rev. A* **59** 3809
[10] Blondel C, Delsart C and Goldfarb F 2001 *J. Phys. B* **34** L281
[11] Osterwalder A, Nee M J, Zhou J and Neumark D M 2004 *J. Chem. Phys.* **121** 6317
[12] Wang D H, Xu Q, Yang C L, Wang M S and Ma X G 2008 *J. Chem. Phys.* **129** 104310
[13] Xing X P, Wang X B and Wang L S 2009 *J. Chem. Phys.* **130** 074301
[14] Du M L 1989 *Phys. Rev. A* **40** 4983
[15] Bracher C, Kramer T and Delos J B 2006 *Phys. Rev. A* **73** 062114
[16] Bracher C and Delos J B 2006 *Phys. Rev. Lett.* **96** 100404
[17] Gao S, Yang G C, Lin S L and Du M L 2007 *Eur. Phys. J. D* **42** 189
[18] Tang T T and Wang D H 2010 *J. Phys. Chem. C* **115** 20529
[19] Wang D H 2014 *J. Electromagnet. Wave.* **289** 861
[20] Huang K Y and Wang D H 2010 *Acta Phys. Sin.* **59** 932 (in Chinese)
[21] Bracher C and Gonzalez A 2012 *Phys. Rev. A* **86** 022715
[22] Wang D H 2013 *J. Electron. Spectrosc.* **189** 96
[23] Zhao L B and Delos J B 2010 *Phys. Rev. A* **81** 053417
[24] Yang B C and Robicheaux F 2015 *Phys. Rev. A* **92** 063410
[25] Yang B C and Robicheaux F 2016 *Phys. Rev. A* **93** 053413
[26] Wang D H, Chen Z H and Cheng S H 2016 *J. Phys. B: At. Mol. Opt. Phys.* **49** 205001
[27] Wang D H, Xu Q F and Du J 2017 *Eur. Phys. J. D* **71** 77
[28] Wang D H 2017 *J. Electron. Spectrosc.* **214** 20
[29] Wang D H, Xu Q F and Ma X G 2017 *Phys. Rev. A* **95** 043410
[30] Wang D H and Wang C J 2017 *Chin. Phys. B* **26** 103202